Asociación Argentina
de Mecánica Computacional

Mecánica Computacional Vol XXX, págs. 1809-1831 (artículo completo)
Oscar Möller, Javier W. Signorelli, Mario A. Storti (Eds.)
Rosario, Argentina, 1-4 Noviembre 2011

EROSION CRITERIA FOR FRICTIONAL MATERIALS UNDER BLAST LOAD

Bibiana Luccioni[a], **Gabriel Aráoz**[b]

[a]*CONICET, Instituto de Estructuras "Arturo M. Guzmán", Universidad Nacional de Tucumán, Av. Independencia 1800, 4000 S.M. de Tucumán, Argentina, bluccioni@herrera.unt.edu.ar,*
http://www.herrera.unt.edu.ar/iest/

[b]*Instituto de Estructuras "Arturo M. Guzmán", Universidad Nacional de Tucumán, Av. Independencia 1800, 4000 S.M. de Tucumán, Argentina, garaoz@herrera.unt.edu.ar,*
http://www.herrera.unt.edu.ar/iest/

Keywords: Hydrocode, concrete, Lagrange, mesh distortion, erosion.

Abstract. Detonation is a type of reaction of the explosive that produces shock waves of great intensity. If the explosive is in contact near a solid material, the arrival of the explosive wave to the surface of the explosive generates intensive pressure waves that can produce the crushing or the disintegration of the material. This shock effect is known as brisance effect. If the explosive is surrounded by air, a pressure wave that can fracture masonry and concrete structures is generated. Both brisance effect and fracture produce discontinuities in the material.
In order to reproduce this type of effects with hydrocodes, an erosion model can be used to remove from the calculus the cells that have reached certain criteria based on deformations. This erosion model represents a numerical remedial to great distortion of Lagrange meshes that can cause excessive deformation of the mesh. For this reason, its application to the simulation of a physical phenomenon requires the calibration with experimental results.
On the other side, erosion criterion and erosion limit used in Lagrange simulations have been found to be important points to study because not only the dimensions of the rupture zone but also the stability of the numerical solution strongly depends on them. A review of different erosion criteria and erosion limits used by different authors to simulate concrete under blast loads is presented in this paper. An application example is developed to show the effect of erosion limit on damage results and the dependence on mesh size. Comparison with experimental results of concrete elements subjected to blast loads is also included in the paper.

1 INTRODUCTION

Concrete has been used extensively to construct civilian buildings, dams, nuclear reactor containment and various defense structures. Therefore, it is important to investigate its behaviors under blast and impact loadings that cause large strains, high strain rates, spalling, fracture and crushing phenomena (Lian et al, 2011).

An explosion in contact or very close to a concrete element is likely to cause a localized shear failure before the wall or column has time to respond to loading in a flexural mode. Localized back face spalling can take place but a breach of the wall or the column could occur due to a shear failure (Millard et al 2010). An explosion at a small distance from a concrete wall will cause a high-speed pressure wave to the front face of the wall. Part of the blast wave energy will be reflected back and a significant proportion will propagate through the wall as a compressive stress wave. When this wave reaches the back face another reflection will take place leading to a tension rebound that can cause back face spalling. Concrete fails in tension and particles are ejected from the back surface at high speed (Millard et al 2010). An explosive loading originated from a greater standoff location could cause failure in flexure of the entire concrete section

Numerical simulation is usually used for predicting the response of these types of structures to blast or impact loads since experimental studies are usually expensive and time consuming. Hence, a lot of effort has been devoted to model the dynamic response of concrete (Unosson et al, 2002; Lian et al, 2011; Rabczuk et al, 2006; Tu and Lu, 2009, 2010; Zhou et al, 2009; Riedel et al, 2010). Moreover, the development of hydrocodes makes possible the simulation of complete blast or impact problems.

Although hydrocodes can analyze problems with both Lagrangian and Eulerian grids, sometimes materials have to be defined using Lagrangian grids even though it is clear that these materials will be subjected to very large distortions arising from gross motion of the Lagrange grid. The element erosion function, while not a material property or physics-based phenomena provides a useful means to simulate the spalling of concrete and provides a more realistic graphical representation of the actual blast events. Erosion is characterized by a physical separation of the eroded solid element from the rest of the mesh (Wu et al, 2011). Though element removal (erosion) associated with total element failure has the appearance of physical material erosion, it is, in fact, a numerical technique used to permit extension of the computation. Without numerical erosion, severely crushed elements in Lagrangian calculations would drive to a very small time step, resulting in the use of many computational cycles with negligible advance in the simulation time. Moreover, Lagrangian elements which have become very distorted have a tendency to “lock up,” thereby inducing unrealistic distortions in the computational mesh (Zukas, 2004).

Erosion function allows removing such Lagrangian cells from the calculation if a pre-defined criterion is reached. When a cell is removed from the calculation process, the mass within the cell can either be discarded or distributed to the corner nodes of the cell. If the mass is retained, conservation of inertia and spatial continuity of inertia are maintained. However the compressive strength and internal energy of the material within the cell are lost whether or not the mass is retained. Erosion causes losses of internal energy, strength and (possibly) mass, therefore erosion limits should be chosen so that cells are not discarded (eroded) until they are severely deformed and their compressive strength and/or mass are not likely to affect the overall results (ANSYS, 2009).

It is important to remark that, in general, although erosion could be used to model actual material erosion it is not true modeling of a physical phenomena, but a numerical solution to overcome problems associated with the excessive mesh distortions. In absence of

experimental evidence it is generally recommended to perform calculus with variable erosion limits to evaluate the effect of erosion limit on numerical results and to use limiting values as high as practicable.

The objective of this paper is the study of the erosion effect on the numerical solution of concrete elements under blast loads. First different available erosion criteria are presented together with the values of erosion limits used by different authors for the numerical simulation of concrete elements under blast or impact load. An application example is presented to show the variability of numerical results with erosion limit and mesh size and to prove that erosion limit based on strain values can not be fixed independently of the mesh size.

2 EROSION MODELS

A summary of different erosion criteria and limits used for the numerical simulation of concrete that can be found in recent papers is included.

The most commonly used commercial codes for the numerical simulation of impact and blast action on concrete elements are AUTODYN (ANSYS, 2009) and LS_DYNA (LS-DYNA, 2003). The erosion criteria available in these codes and generally used by different authors are presented in this section.

Additionally, other techniques used to avoid using erosion are also mentioned in this section. The section is completed with some comments about the great dispersion in erosion values found in literature.

2.1 Summary of Erosion Criteria and limits used by different authors

The erosion criteria and limit values used by different authors to simulate concrete, reinforced concrete, fiber reinforced concrete (FRC) and high performance fiber reinforced concrete (HPFRC) in recent papers are summarized in Table 1 where the corresponding references are also included.

Problem	Material	Criteria	Limit	Program	Mesh size	Reference
Blast	Concrete 40MPa	Principal strain	0.01	LS-DYNA	18.75x18.75 x25mm	Xu K. and Lu Y. (2006)
Blast	Concrete 35Mpa	Instantaneous Geometric strain	-2	AUTODYN	12x12x6mm 6x6x6mm	Nyström U. and Gylltoft (2009)
Blast	Conc: Mortar 48MPa, Agg150MPa)	Tensile damage	0.9	AUTODYN	2mm	Zhou and Hao (2009)
Blast	Concrete 24MPa	Principal strain	0.15	LS-DYNA	50mm	Shi et al (2010)
Blast	Concrete 24MPa	Shear strain	0.9	LS-DYNA	50mm	Shi et al (2010)
Blast	Concrete 60MPa	Tensile Stress	5MPa	LS-DYNA	6.25 to 100mm	Tang and Hao (2010)
Blast	Concrete 60MPa	Principal strain	0.1	LS-DYNA	6.25 to 100mm	Tang and Hao (2010)
Blast	Concrete 40MPa	Max strain	0.1	LS-DYNA	50mm	Wu et al (2011)
Blast	FRC 1% 28MPa	Shear strain	0.4	LS-DYNA		Wang et al (2009)
Blast	FRC 1% 28MPa	Tensile Stress	5.4MPa	LS-DYNA		Wang et al (2009)

Blast	FRC 1.5% 30Mpa	Shear strain	0.4	LS-DYNA		Wang et al (2009)
Blast	FRC 1.5% 30Mpa	Tensile Stress	6.0MPa	LS-DYNA		Wang et al (2009)
Blast	FRC 2% 32MPa	Shear strain	0.4	LS-DYNA		Wang et al (2009)
Blast	FRC 2% 32MPa	Tensile Stress	7.5 MPa	LS-DYNA		Wang et al (2009)
Blast	FRC 45MPa	Damage	0.99	LS-DYNA	25x25mm	Cuoghlin et al (2010)
High vel impact	Concrete 25MPa	Geometric strain	2.5	AUTODYN	2.5mm	Bepu et al (2008)
High Dynamic	Concrete 35MPa	Principal tensile strain	0.002	LS-DYNA AUTODYN	6 a 8mm	Tu and Lu (2009)
Impact	Concrete (mortar+aggr.)	Instantaneous Geometric strain	-0.05 mort - 0.03 aggr	AUTODYN	0.5x0.5mm	Hao et al (2010)
Impact	Concrete 37.7MPa	Geometric strain	-2	AUTODYN	0.2mm	Riedel et al (2009)
Impact	Concrete 40MPa	Strain limit	1.5			Tu and Lu (2010)
Projectile impact	Concrete 48 a 140MPa	Strain failure	-1 (comp) 0.5 (tens)	LS-DYNA	2mm	Islam et al (2011)
Dynam load	Concrete 30Mpa			LS-Dyna		Song and Lu (2011)
High velocity impact	FRC 28-30-32MPa	Shear strain failure	0.4	LS-DYNA	1.25mm	Teng et al (2008)
High velocity impact	FRC 28-30-32MPa	Tension stress failure	5.4-6.01-7.35 MPa	LS-DYNA	1.25mm	Teng et al (2008)
Projectile impact	FRC asp.ratio 60 95 Mpa	Shear strain	0.4	LS-DYNA	2mm	Wang et al (2010)
Projectile impact	FRC asp. ratio 60 95 Mpa	Tensile Stress	14.3MPa	LS-DYNA	2mm	Wang et al (2010)
Projectile impact	FRC asp. ratio 20 105MPa	Shear strain	0.4	LS-DYNA	2mm	Wang et al (2010)
Projectile impact	FRC asp. ratio 20 105MPa	Tensile Stress	15.75MPa	LS-DYNA	2mm	Wang et al (2010)
Impact	FRC 1% 179.2 Mpa	Max strain	0.0035	LS-DYNA	0.25mm	Wang et al (2010)
Impact	FRC 2% 191.7Mpa	Max strain	0.0035	LS-DYNA	0.25mm	Wang et al (2010)
Low velocity impact	HPFRC	Ultimate shear strain	0.012	LS-DYNA	6 to 8mm	Farnam et al (2010)
Proyectile impact	Concrete and HRF 33.8Mpa	Instantáneous Geometric strain	-1.5	AUTODYN	5mm	Nyström and Gylltoft(2011)

Table 1: Different erosion criteria and erosion limits used in recent papers.

2.2 Erosion Criteria

The different erosion criteria available in the literature can be classified according to the type of variable used to control erosion.

2.1.1. Strain based

- Instantaneous geometric strain (ANSYS, 2009): Erosion is initiated when an instantaneous geometric strain limit is reached

$$\varepsilon_{eff} \geq \left(\varepsilon_{eff}\right)_{\lim} \tag{1}$$

$$\varepsilon_{eff} = \frac{2}{3}\sqrt{\left(\varepsilon_1{}^2 + \varepsilon_2{}^2 + \varepsilon_3{}^2\right) + 5\left(\varepsilon_1\varepsilon_2 + \varepsilon_1\varepsilon_3 + \varepsilon_2\varepsilon_3\right) - 3\left(\varepsilon_{12}{}^2 + \varepsilon_{23}{}^2 + \varepsilon_{13}{}^2\right)} \tag{2}$$

This criterion represents a limit in effective strain, a kind of quadratic norm of the strain tensor. The instantaneous geometric strain can increase or decrease with loading and unloading but once an element has been eroded it can no longer be recovered. It should be noted that this criterion is independent of the strain sign. In this sense it seems to be useful for metals but not adequate to model frictional materials response characterized by a great difference between tension and compression behavior. Nevertheless, this criterion has been successfully used by some authors to model concrete and fiber reinforced concrete under blast loads (Nyström and Gylltoft 2009) and impact load (Hao et al 2010, Beppu et al 2008, Nyström and Gylltoft 2011, Riedel et al 2009, Tu and Lu 2010, Islam et al 2011). Some of these authors distinguish between compression and tension limits (Nyström U. and Gylltoft 2009, Hao et al 2010, Nyström and Gylltoft 2011, Riedel et al 2009, Islam et al 2011) but it is not clear how are effective compression strain and effective tension strain defined. Limit values used for compression are always higher than limit values for tension. In some cases only effective strain in compression is limited and in many cases the erosion limits used for compression are several orders higher than concrete compression strain at failure under high dynamic loads. As a consequence, concrete elements are eroded much after failure

- Maximum principal strain (LS-DYNA, 2003): Erosion is initiated when a maximum principal strain is reached

$$\varepsilon_1 \geq \left(\varepsilon_1\right)_{\lim} \tag{3}$$

The maximum strain can increase and decrease with loading and unloading but like in the preceding case, once the element has been eroded, it can no longer be recovered. This is typically a limit in tension strain. When applied to brittle materials like concrete it can be physically interpreted as a limit in crack opening. It can represent tensile fracture and spalling of concrete under blast and impact loads but it seems useless to represent brisance effect or erosion under high compression stresses.

This criterion has been successfully used by many authors to represent concrete erosion under blast loads (Shi et al 2010, Wu et al 2011, Tang and Hao 2010), concrete under high dynamic loads (Tu and Lu 2009) and FRC under impact load (Wang et al 2010). The values used for the erosion limit in tension are sensible lower than those used for the instantaneous geometric strain and resemble concrete limit strain under tension. Xu K and

Lu Y. (2006) define the erosion by a limit tensile strain that they calculate from static tensile limit strain considering dynamic amplification under blast loads, effect of confinement and reinforcement. Using this approach they obtain a good representation of the phenomenon of spallation of reinforced concrete plates. Nevertheless, they state that more robust criteria for erosion may result in more accurate simulation results

- Maximum shear strain (LS-DYNA, 2003): Erosion is initiated when a maximum principal strain is reached

$$\gamma_1 \geq \left(\gamma_1\right)_{\text{lim}} \tag{4}$$

Like previous erosion limits, the maximum shear strain can increase or decrease with loading/unloading but once an element has been eroded it is eliminated from calculus and it can not be recovered. This criterion can be physically assimilated to shear failure like that obtained in concrete elements subjected to contact explosion or close blast loads or concrete plates under projectile perforation. In all these cases the concrete elements failure is characterized by a local shear failure that takes place before the loads are transmitted to the supports and structural behavior is mobilized. The estimation of the shear strain erosion limit from concrete properties is not straightforward.

Many authors have used this criterion to define erosion of concrete (Sih et al 2010) and FRC (Wang et al 2009) under blast loads and projectile impact and erosion produced by projectile impact (Islam et al 2011, Wang et al 2010, Teng et al 2008) and low velocity impact (Farnam et al 2010) on fiber reinforced concrete plates.

- Incremental geometric strain (ANSYS, 2009): Erosion is initiated when an incremental geometric strain limit is reached

$$\bar{\varepsilon}_{eff} \geq \left(\bar{\varepsilon}_{eff}\right)_{\text{lim}} \tag{5}$$

$$\bar{\varepsilon}_{eff} = \int \dot{\bar{\varepsilon}}^{p}_{eff} dt \qquad \dot{\bar{\varepsilon}}_{eff} = \frac{2}{3}\sqrt{\dot{\varepsilon}_{xx}{}^2 + \dot{\varepsilon}_{yy}{}^2 + \dot{\varepsilon}_{zz}{}^2 + \dot{\varepsilon}_{xy}{}^2 + \dot{\varepsilon}_{xz}{}^2 + \dot{\varepsilon}_{yz}{}^2} \tag{6}$$

Although available in commercial codes this criterion does not seem to be physically consistent with concrete erosion resulting from blast or impact loads. In general, failure, damage and yielding criteria for concrete can not be represented by incremental strains or stress.

No papers using this type of erosion criterion have been found in the literature.

- Effective plastic strain (ANSYS, 2009). Erosion is initiated when an effective plastic strain limit is reached.

$$\varepsilon^{p}_{eff} \geq \left(\varepsilon^{p}_{eff}\right)_{\text{lim}} \tag{7}$$

$$\varepsilon^{p}_{eff} = \int \dot{\varepsilon}^{p}_{eff} dt \qquad \dot{\varepsilon}^{p}_{eff} = \frac{\sqrt{3J_2} - \sigma_y}{3G} \tag{8}$$

J_2: second invariant of the stress deviator

σ_y: uniaxial yield stress

G: shear modulus

This is a plasticity base criterion with the advantage that plastic strains are irreversible and can be physically interpreted as irrecoverably deformations. Eq. (8) defines a J_2 plastic flow, normally used in hydrocodes where hydrostatic and deviatory responses are decoupled. Nevertheless, a more complex plastic flow can be used. Although physically more founded, no references using this type of erosion criterion for concrete under impact or blast loads have been found.

The independence of the mesh size should be checked when strain based erosion criteria are used in combination with finite element method.

2.1.2. Stress based

Stress based erosion criteria (LS-DYNA, 2003) are similar to yield criteria in classical plasticity. The strength enhancement due to high strain rates should be taken into account in the stress-based erosion limits.

Different ways of defining the stress erosion limit can be found.

- Pressure: Erosion is initiated when a maximum (minimum) pressure is reached,

$$p \geq p_{\lim} \quad \text{or} \quad p \leq p_{\min} \tag{9}$$

When used in tension, this erosion criterion is similar to tension cut off in classical plasticity or hydro tensile limit. No references using this erosion limit have been found.

- Principal stress: Erosion is initiated when maximum principal stress reaches a limit

$$\sigma_1 \geq (\sigma_1)_{\lim} \tag{10}$$

This criterion can be physically assimilated to a limitation of tension stresses and the values of the stress limit can be derived from tension strength of concrete.

This criterion has been used to model concrete (Tang and Hao 2010) and fiber reinforced concrete (Wang et al 2009) under blast loads and fiber reinforced concrete under projectile impact (Wang et al 2010, Teng et al 2008).

- Effective stress: Erosion is initiated when effective stress reaches a limit

$$\sigma_{eff} \geq (\sigma_{eff})_{\lim} \tag{11}$$

$$\sigma_{eff} = \sqrt{\frac{2}{3}\sigma_{ij}\sigma_{ij}} \tag{12}$$

This a typically J_2 based criterion for metallic materials. Although available in hydro codes it is no suitable for frictional materials like concrete.

2.1.3 Damage based

- Damage (LS-DYNA, 2003): Erosion is initiated when damage limit is reached

$$D \geq (D)_{\lim} \tag{13}$$

This criterion seems to be adequate and physically founded. Damage used as erosion indicator is an always increasing variable, generally associated with stiffness degradation. Nevertheless, it should be noted that this type of criteria are strongly related to the constitutive model used for concrete. A model considering damage should be used and depending on the type of damage model, different definitions of the damage variable and its evolution can be found.

Zhou et al (2009) have used a tensile damage criterion to model concrete under blast loads using a micro mechanical approach. Cuoghlin et al (2010) used a damage criterion to model erosion in fiber reinforced concrete under impact loads.

2.1. 4 Failure

All the preceding erosion criteria can be considered as failure criteria. Other failure criteria that are available in commercial codes to define erosion are presented in this section. No use of this type of criteria has been found in the specialized literature.

- Failure (ANSYS, 2009): Erosion is initiated after element failure. For example when Tuler-Butcher criterion (LS-DYNA, 2003) is reached:

$$\int_0^t \left[\max(0, \sigma_1 - \sigma_o)\right]^2 dt \geq K_f \tag{14}$$

σ_o is a specified threshold stress

K_f is a the stress impulse at failure

2.1.5 Other

- Timestep (ANSYS, 2009): Erosion is initiated when a minimum element timestep is reached

$$\Delta t \leq \Delta t_{\lim} \tag{15}$$

This type of criterion has no physical meaning and it seems arbitrary in the case of concrete elements under blast or impact loads.

2.3 Alternative procedures

To avoid using erosion technique, Wang et al (2009) present a method based on continuum damage mechanics and mechanics of micro-crack development. The fragmentation process is modeled according to the crack initiation and propagation, which depend on the material damage levels.

Alternatively, Riedel et al (2010) stop the simulation when the damage is fully established but when the damaged material is still mostly in place. Cells extremely damaged are deleted in problem visualization showing the same aspect as that achieved with erosion criteria and avoiding too long simulations.

All the works mentioned in previous section and above are conducted by finite element method (FEM), in which erosion method with some element deleted must be implemented to capture the phenomenon of perforation. Meshfree/meshless and particle methods have been developed and received considerable attention during last decades (Lian et al, 2011). A representative of such methods is the material point method (MPM), which is an extension of the fluid implicit particle (FLIP) method to solid mechanics. MPM discretizes a material

domain by a set of Lagrangian material points (particles) moving through an Eulerian background grid. The numerical dissipation normally associated with Eulerian methods is removed, while mesh distortion and element entanglement associated with the Lagrangian finite element method are avoided (Lian et al, 2011).

2.4 Remarks

It can be proved that different solutions are obtained for different erosion limits. Moreover, the fragility curve determination for an extreme damage level (collapse) is described by Aráoz and Luccioni (2008) from a numerical analysis of masonry walls under blast loads considering the uncertainty of the material erosion limit. The important variability observed in the results obtained showed the importance and need of further research relative to erosion criteria and limits. These results and conclusion can be extrapolated to concrete.

Commercial software usually recommends the calibration with experimental results and the use of as high as possible erosion limits, but it is clear that this suggestion cannot be used to model actual erosion of concrete.

Numerous criteria have been used to simulate different types of concrete elements under explosive and impact loads. Additionally some authors use two erosion criteria simultaneously so that the one that is first reached activates erosion.

It is difficult to state which is the best erosion criterion from the summary of results presented in Section 2.1. Some general guides have been provided in Section 2.2. It seems that erosion criteria should be appropriate to reproduce the type of failure expected.

Generally all authors have calibrated erosion limits to reproduce the experimental results that correspond to different physical problems: contact blast, near field blast, distant blast, projectile impact, low velocity impact, etc. They show good results for the problems simulated. Most criteria are based on strain limits. The limit values used by different authors (Table 1) are extremely different even for similar material properties and mesh size.

Authors usually adjust materials properties with experimental results and then use the corresponding properties to solve other problems. Nevertheless, it should be proved if that erosion limit is a material property independent of the mesh size. Moreover, the question is how to decide the best erosion criterion and limit in order to simulate a specific problem whose type of failure is not previously known.

3 APPLICACTION EXAMPLE

3.1 Introduction

The study of the effect of erosion criterion and limits on the numerical results is developed in this section based on applications related to a concrete slab subjected to contact blast load.

All the numerical analysis is performed with the hydrocode ANSYS Autodyn (2009). An Euler Godunov multi material with strength higher order processor is used to model the air and the explosive while a Lagrange processor is used for concrete.

The ideal gas equation of state is used for the air. Lee-Tarver equation of state (Lee and Tarver, 2008) is used to model both the detonation and expansion of TNT in conjunction with “Jones - Wilkins - Lee” (JWL EOS) to model the unreacted explosive. An elastoplastic model is used for steel and RHT model is used for concrete.

3.2 Concrete plate under contact blast load

A concrete slab tested under blast loading by Rabzuk and Eibl (2006) is modeled. This slab has also been modeled by Zhou et al (2009). The dimensions of the tested slab are 1.2mx1.2mx0.32m and the concrete compression strength is 48 MPa. The slab is supported at its corners and loaded by an explosive cone of TNT and Composition B. The equivalent charge weight is about 350 g. The inner cone consisted of TNT and the outer thin cone of composition B. A scheme of the tested slab with the dimensions in mm is shown in Fig. 1. More details about this experimental test can be found in the paper by Rabzuk and Eibl (2006).

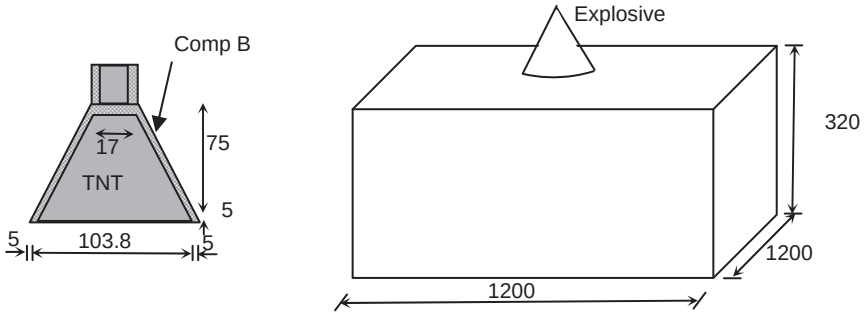

Figure 1: Test layout (Dimensions in mm)

The damaged plate after the explosion is shown in Figure 2.

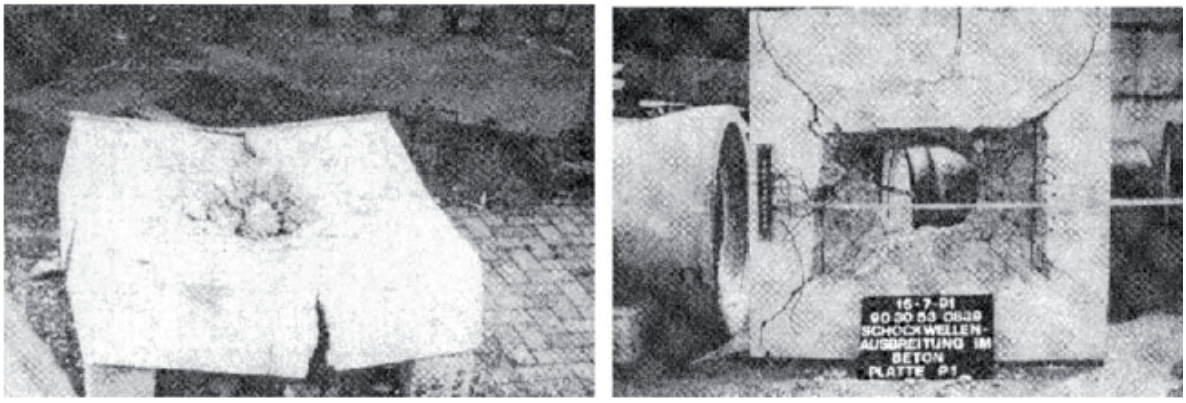

Figure 2: Damaged slab (Rabczuk and Eibl 2006) a) Top view; b) Bottom view

3.3 Numerical simulation

The numerical model used to simulate this problem is represented in Figure 3. Due to symmetry conditions only one fourth of the slab is actually modeled. The model contains the air volume where the slab is immersed and where the explosive is detonated and the slab itself. As the explosive is in contact with the slab the mesh is refined in coincidence with explosive charge to guarantee a minimum of ten elements inside explosive in each direction. Initially a 2mm cell size is used for the slab.

Air flow is allowed in the air mesh sides and the slab is supposed to be fixed in its corners. Euler-Lagrange interaction is defined.

The problem is run until no more deformation or erosion occurs.

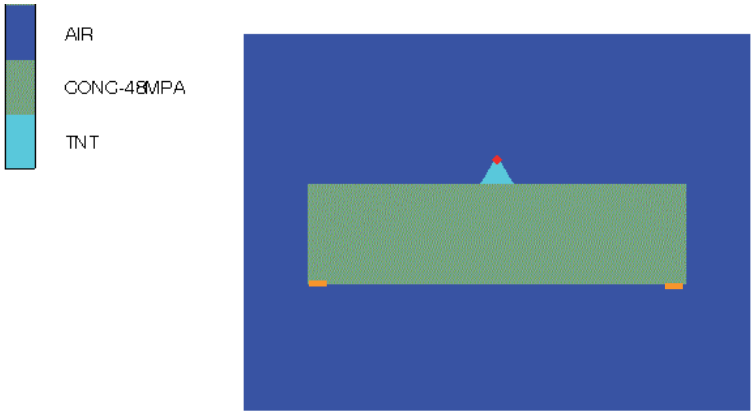

Figure 3: Numerical model for the slab

3.4 Concrete model

A RHT model (Riedel et al, 1999) with a P-alpha equation of state (Herrman 1969) is used for concrete.

As the analysis is performed with a hydrocode, an equation of state(EOS) is required to describe the material behavior, in addition to the constitutive model. The equation of state links together three inter-independent thermodynamic variables: pressure p, density ρ and the specific internal energy e.

A p-α equation of state (Herrmann, 1969) is used for concrete. This EOS has been proved to be capable of representing well the concrete thermodynamic behavior at high pressures and it also allows for a reasonably detailed description of the compaction behavior at low pressure ranges (Tu and Lu, 2009). It assumes that the initial specific internal energy for the porous material is the same as the solid material under the same pressure and temperature.

The equation of state of the fully compacted or solid material is described with a polynomial function as,

$$p = A_1\,\mu + A_2\,\mu^2 + A_3\,\mu^3 + \left(B_0 + B_1\,\mu\right)\rho_0\,e \qquad \text{for } p \geq 0 \text{ (compactation)}$$

$$p = T_1\,\mu + T_2\,\mu^2 + B_0\,\rho_0\,e \text{ for } p < 0 \tag{16}$$

where A_i, B_i and T_i are coeficients, ρ_0 is the inicial density and

$$\mu = \frac{\rho}{\rho_0} - 1 \tag{17}$$

is the relative volume change.

The EOS for the porous material is calculated by substituting a new variable $\alpha\rho_p$ for ρ in Eq. (17) and Eq. (16), i.e.,

$$p = A_1\,\bar{\mu} + A_2\,\bar{\mu}^2 + A_3\,\bar{\mu}^3 + \left(B_0 + B_1\,\bar{\mu}\right)\rho_0\,e \text{ for } p \geq 0 \tag{18}$$

$$\bar{\mu} = \frac{\alpha \rho_p}{\rho_0} - 1 \tag{19}$$

Where ρ_p is the density of the porous material and α a is called material ‘‘porosity’’ that can be defined as

$$\alpha = \frac{\rho_s}{\rho_p} \tag{20}$$

where ρ_s and ρ_p refer to the density of the solid and the porous material at the same pressure and temperature respectively . In the p-α equation of state the following definition is used,

$$\alpha(p) = 1 + (\alpha_{init} - 1)\left(\frac{p_{lock} - p}{p_{lock} - p_{crush}}\right)^n \tag{21}$$

Where α_{init} is the initial porosity of the intact concrete; p_{crush} corresponds to the pore collapse pressure beyond which concrete plastic compaction occurs and p_{lock} is the pressure at which the concrete porosity α reaches unity.

The RHT strength model (Riedel et al, 1999) is a combined plasticity and shear damage model in which the deviatoric stress $Y = \sqrt{3J_2}$ is limited by a generalized failure surface defined as

$$\left(\sqrt{3J_2}\right)_{fail} = Y_{fail}\left(p^*, \theta, \dot{\varepsilon}\right) = Y_C\left(p*\right) r_3(\theta) F_{rate}\left(\dot{\varepsilon}\right) \tag{23}$$

$$Y_c\left(p^*\right) = f_c\left[A\left(p^* - p^*_{spall}\ F_{rate}\left(\dot{\varepsilon}\right)\right)^N\right] \tag{24}$$

Where f_c is the uniaxial compression strength; A and N are material constants; $p^*=p/f_c$ is the normalizad pressure, p is the hydrostatic pressure and $p^*_{spall} = f_t / f_c$, where f_t is the uniaxial tension strength; $F_{rate}\left(\dot{\varepsilon}\right)$ represents the dynamic amplification factor (DIF) as a function of strain rate $\dot{\varepsilon}$.

$$r_3(\theta) = \frac{r}{r_c} \tag{25}$$

$$r_3(\theta) = \frac{2\left(1-\psi^2\right)\cos\theta + (2\psi - 1)\sqrt{4\left(1-\psi^2\right)\cos^2\theta + 5\psi^2 - 4\psi}}{4\left(1-\psi^2\right)\cos^2\theta + (1-2\psi)^2} \tag{26}$$

$$\cos 3\theta = \frac{3\sqrt{3}}{2}\frac{J_3}{\left(J_2\right)^{3/2}} \tag{27}$$

$$\psi = \frac{r_t}{r_c} = Q + BQp^* \tag{28}$$

J_2 and J_3 represent the second and the third invariants of the devaitoric stress tensor. Figure 4 shows the intersections of the failure surface with different deviatoric planes. The input parameter Q defines the ratio of strength at zero pressure and the coefficient BQ defines the rate at which the fracture surface transitions from an approximately triangular form to a circular form with increasing pressure.

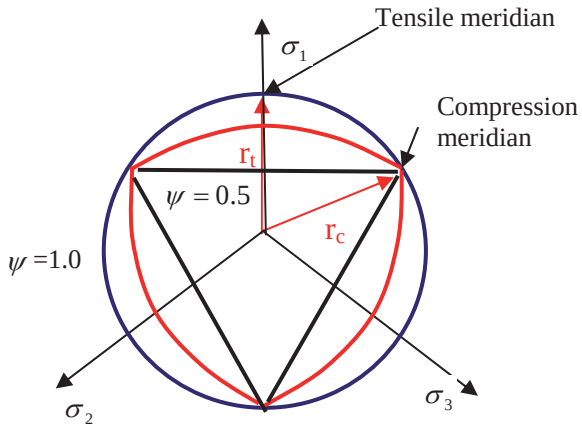

Figure 4: Typical failure curves in a deviatoric plane for different hydrostatic pressures

Strain rate effects are represented through increases in fracture strength with plastic strain rate. Two different terms can be used for compression and tension with linear interpolation being used in the intermediate pressure regime.

$$F_{Rate} = \begin{cases} 1 + \left(\dfrac{\dot{\varepsilon}}{\dot{\varepsilon}_0}\right)^{\alpha} & \text{for } p > \frac{1}{3} f_c \text{ (compression)} \\ 1 + \left(\dfrac{\dot{\varepsilon}}{\dot{\varepsilon}_0}\right)^{\delta} & \text{for p} < \frac{1}{3} f_t \text{ (tension)} \end{cases} \tag{29}$$

δ is the compression strain rate factor and α is the tension strain rate factor.

Strain hardening is represented in the model through the definition of an elastic limit surface and a "hardening" slope. The elastic limit surface is scaled down from the fracture surface

$$Y_{elast} = Y_{fail}\left(p^*\right) F_{elast}\ F_{cap}\left(p\right) \tag{30}$$

F_{elas} is the ratio of the elastic strength to failure surface strength derived from two input parameters (elastic strength/f_c) and (elastic strength/f_t). The pre-peak fracture surface is

subsequently defined through interpolation between the elastic and fracture surfaces using the "hardening" slope $\frac{G_{elas}}{G_{elas} - G_{plas}}$.

The model presents the option of including a cap to limit the elastic deviatoric stress under large compressions. This option effectively leads to the assumption that porous compaction results in a reduction in deviatoric strength.

The elastic, fracture and residual failure surfaces are shown schematically in Fig.5.

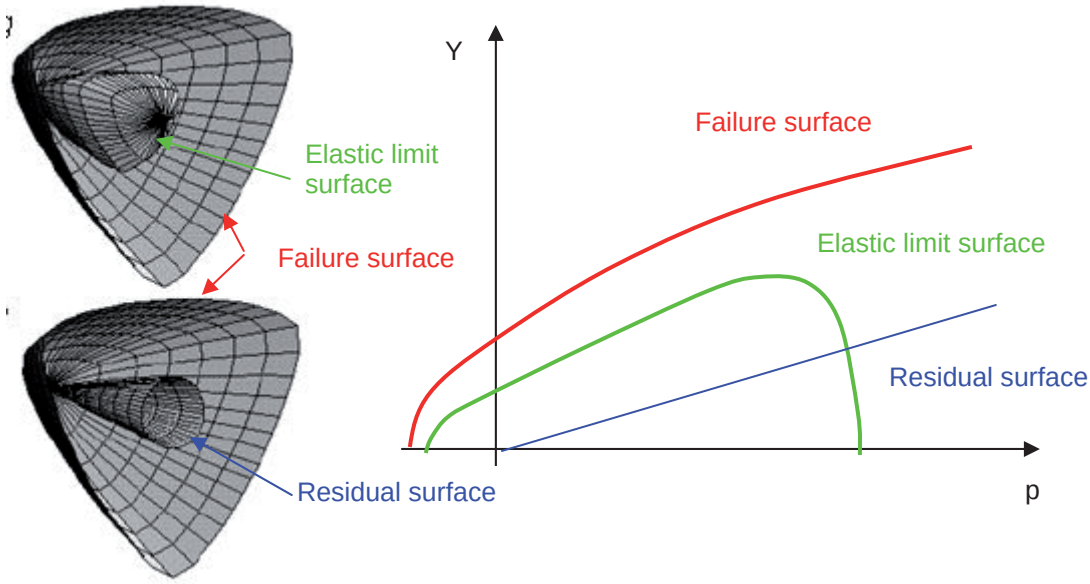

Figure 5: Elastic, fracture and residual surfaces

A residual (frictional) failure surface is defined as,

$$Y^*_{resid} = B\, p^{*M} \tag{31}$$

Where B is the residual failure surface constant and M is the residual failure surface exponent, both input parameters.

Damage is assumed to accumulate due to inelastic deviatoric straining (shear induced cracking) using the relationships

$$D = \sum \frac{\Delta \varepsilon_{pl}}{\varepsilon_p^{fail}}$$
$$\varepsilon_p^{fail} = D_1 (p^* - p^*_{spall})^{D_2} \tag{32}$$

where D_1 and D_2 are material constants used to describe the effect strain to fracture as a function of pressure.

Damage accumulation can have two effects in the model

- Strain softening (reduction in strength). The current fracture surface (for a given level of damage) is scaled down from the intact surface

$$Y^*_{fract} = (1-D)Y^*_{fail} + DY^*_{resid} \tag{33}$$

- Reduction in shear stiffness

$$G_{frac} + (1-D)G_{elas} + DG_{resid} \tag{34}$$

The material properties used are presented in Table 2.

3.5 Effective strain erosion criterion

Instantaneous geometric strain is used as erosion criterion in this section. Following the usual recommendations, erosion limit is varied in order to obtain a numerical solution that correlates to experimental results in terms of physical erosion.

Figure 6 shows the damage obtained with a 2mm cell size for different erosion limits. The dimensions of the slab perforation obtained are presented in Table 3 together with experimental results (Rabzuk and Eibl, 2006). From Figs 2 and 6 and Table 3 it is clear that in this case the more appropriate value for the erosion geometric strain limit is 0.001.

All the examples presented in Fig. 6 correspond to a 2mm mesh size for the plate. In order to study the relation between the erosion limit and the mesh size the same problem is solved but with a coarser mesh (10mm). First the erosion limit is taken as 0.001. The resulting damage is presented in Fig.7a and does not represent the actual damage. As done for the finer mesh, erosion limit value is varied in order to obtain the damage pattern observed in the test (Rabzuk and Eibl, 2006). The corresponding damage patterns and crater diameters obtained are presented in Fig.7 and Table 3 respectively. From Fig. 7 and Table 3, it seems that actual damage is better modeled with an erosion limit of 0.0002. This erosion value can be obtained based on an analogy with the procedure used to obtain mesh size objectivity when finite element method is used in combination with strain softening models. Nevertheless it should be noted that for this value the crater is rather bigger than the crater found in the experiment (Rabzuk and Eibl, 2006).

If an even coarser mesh it used, the erosion limit should be corrected to obtain the same damage pattern. Fig.8 shows the crater obtained with a 40mm mesh size, following the same rule that is, with an erosion limit of 0.00005. It is clear that in this case the crater is bigger than that obtained in the test.

It should be observed that damage pattern is strongly dependent not only on erosion limit but also on mesh size. This conclusion suggests that strain based erosion limit can not be independent of mesh size.

3.6 Other erosion criteria

In order to analyze the behavior of different erosion criteria, the same problem is solved but with other erosion criteria and the results are compared with those obtained in previous section and with experimental results.

Equation of State P alpha		**Strength RHT Concrete**	
Reference density	2.75 g/cm^3	Shear Modulus	8.30E+06 kPa
Porous density	2.33 g/cm^3	Compressive Strength (f_c)	4.80E+04 kPa
Initial compaction pressure	2.40E+04 kPa	Tensile Strength (f_t/f_c)	8.30E-02
Solid compaction pressure	2.50E+05 kPa	Shear Strength (f_s/f_c)	1.80E-01
Compaction exponent	3.00E+00	Intact Failure Surface Constant A	1.60
Solid EOS	Polynomial	Intact Failure Surface Expon. N	6.10E-01
Bulk Modulus A1	3.527E+07 kPa	Tens./Comp. Meridian Ratio (Q)	6.805E-01
Parameter A2	3.958E+07 kPa	Brittle to Ductile Transition	1.05E-02
Parameter A3	9.04E+06 kPa	G (elas.)/(elas.-plas.)	2.00E+00
Parameter B0	1.22E+00	Elastic Strength / ft	7.00E-01
Parameter B1	1.22E+00	Elastic Strength / fc	5.30E-01
Parameter T1	3.527E+07 kPa	Fractured Strength Constant B	1.60E+00
Parameter T2	0.00E+00 kPa	Fractured Strength Exponent M	6.10E-01
Compaction Curve	Standard	Compressive Strain Rate Exp. α	3.20E-02
		Tensile Strain Rate Exp. δ	3.60E-02
		Max. Fracture Strength Ratio	1.00E+20
		Use CAP on Elastic Surface?	Yes
		Failure RHT Concrete	
		Damage Constant, D1	4.00E-02
		Damage Constant, D2	1.00E+00
		Minimum Strain to Failure	1.00E-02
		Residual Shear Modulus Fraction	1.30E-01
		Tensile Failure	Hydro (Pmin)

Table 2: Concrete properties

a)

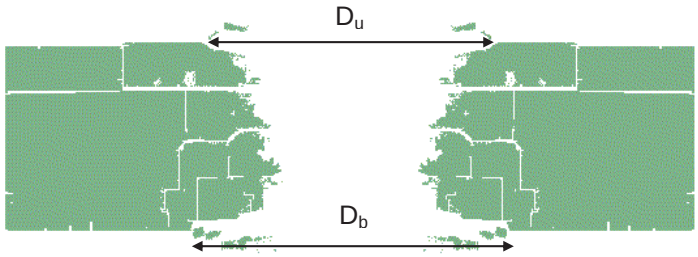

b)

c)

Figure 6: Damaged slab (Numerical simulation for a 2mm mesh size) for different erosion limits.

a) $\left(\varepsilon_{eff}\right)_{\lim} = 1E-3$, b) $\left(\varepsilon_{eff}\right)_{\lim} = 1E-2$, c) $\left(\varepsilon_{eff}\right)_{\lim} = 1E-1$

3.6.1. Plastic strain

The results obtained using a 2mm mesh size for the plate and a plastic strain based erosion criterion taking $\left(\varepsilon_{eff}^{p}\right)_{\lim} = 0.001$ are coincident with those obtained with effective strain criterion and the same limit presented in Fig.6a and Table 3. Elastic extension of concrete is small when compared to plastic strain so the difference between total strain and plastic strain practically does not affect the final erosion.

3.6.2. Principal stress

The results obtained using a 2mm mesh size for the plate and a principal stress based erosion criterion are presented in Fig.9a and Table 3. These results correspond to an erosion limit defined as $\sigma_1 \geq \left(\sigma_1\right)_{\lim} = f_t$. It can be seen that, although strain rate strength increment was not taken into account, the numerical model approximately reproduces the damage observed in the experiment. Nevertheless the shape of the perforation is better reproduced using a strain based erosion criteria.

a)

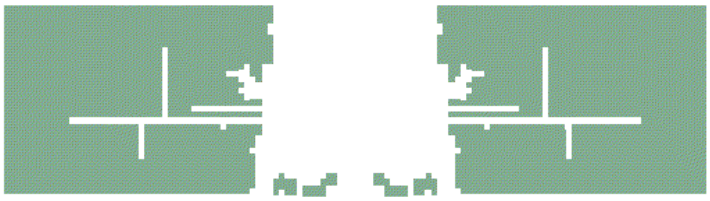

b)

c)

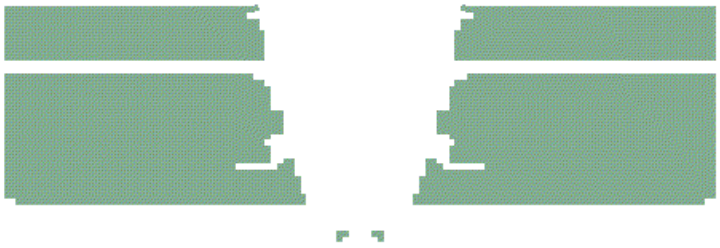

Figure 7: Damaged slab (Numerical simulation 10mm mesh size). a) $\left(\varepsilon_{eff}\right)_{\lim} = 1E-3$; b) $\left(\varepsilon_{eff}\right)_{\lim} = 2E-4$; c) $\left(\varepsilon_{eff}\right)_{\lim} = 5E-3$

Figure 8: Damaged slab (Numerical simulation 40mm mesh size, $\left(\varepsilon_{eff}\right)_{\lim} = 5E-5$

	Upper crater Diameter D_u(mm)	Bottom crater Diameter D_b(mm)
Experiment (Zhou et al 2008)	510	620
Numer. 2mm $\left(\varepsilon_{eff}\right)_{\lim} = 1E-3$	520	570
Numer. 2mm $\left(\varepsilon_{eff}\right)_{\lim} = 1E-2$	370	---
Numer. 2mm $\left(\varepsilon_{eff}\right)_{\lim} = 1E-1$	240	---
Numer 10mm $\left(\varepsilon_{eff}\right)_{\lim} = 1E-3$	290	370
Numer 10mm $\left(\varepsilon_{eff}\right)_{\lim} = 2E-4$	560	720
Numer 10mm $\left(\varepsilon_{eff}\right)_{\lim} = 5E-3$	360	220
Numer 40mm $\left(\varepsilon_{eff}\right)_{\lim} = 5E-5$	720	670
Numer. 2mm $\left(\varepsilon_{eff}^{p}\right)_{\lim} = 0.001$	520	570
Numer. 2mm $\left(\sigma_1\right)_{\lim} = 4.8MPa$	620	620
Numer. 2mm RHT Damage failure B=1.6 , $D_1 = 0.04$, $D_2 = 1$	178	----
Numer. 2mm RHT Damage failure B=0.16 , $D_1 = 0.004$, $D_2 = 1$	260	----
Numer. 2mm p_{min}=0 failure	272	-----

Table 3: Summary of experimental and numerical results for crater dimensions

3.6.3. Damage based failure

The same problem is simulated with a 2mm mesh size and an erosion criterion based on failure. RHT uses a damage based criterion (Eqs. (31) and (32)) to define failure. If the default values are used for the parameters describing damage, that is B=1.6 $D_1 = 0.04$ and , $D_2 = 1$ the erosion observed in the test can not be reproduced, see Fig.10 and Table 3. If the parameters defining the fracture surface are modified, the resulting crater is enlarged but physical erosion observed in the test can not be reproduced. The results are presented in Fig.10b and Table 3.

3.6.4. p_{min} based failure

If the problem is solved with a 2mm mesh size and an erosion criterion based on failure defined by $p_{\min} = 0$, the results presented in Fig.11a and Table 3 are obtained. It is clear that, like in previous case, actual erosion can not be reproduced using this criterion. As illustration the plastic zones obtained in this case are presented in Fig.11b. It can be seen that plastic zones approximately reproduce the eroded zone.

4 CONCLUSIONS

A review of erosion algorithm frequently used in numerical simulations of blast and impact loading on concrete elements is presented. Erosion algorithms are numerical solutions to avoid great mesh deformation when Lagrange processors are used. Nevertheless, in the case of concrete they can be used to represent physical erosion, shear failure, cratering, spalling and fracture.

The review presented shows a great dispersion of erosion criteria and erosion limits used by different authors for similar types of concrete. The differences found suggest that erosion limit requires further research.

The review presented also shows that erosion criteria should be adequate to the type of "physical erosion" phenomena that is intended to be modeled. Although very simple, erosion criteria based on strain limits can be more easily related to physical phenomenon occurring in concrete under blast and impact loads. The review presented and the example developed show that this criterion is able to reproduce concrete failure under close blast loads.

Numerical results are dependent on the erosion limit used. The use of erosion limits as high as possible is usually recommended in classical software used for the numerical simulation of blast or impact loads. The need of calibration with experimental results is also stated. What is not well established is if this erosion limit should be considered as a material property or not.

The application example developed in this paper includes comparison with experimental results and proves that erosion limit is not independent of mesh size, thus it can not be considered as a material property. It is normally expected to obtain different results when the same problem is solved with different mesh sizes. Nevertheless the difference tends to disappear when the mesh is refined. If strain based erosion criteria is considered another type of mesh size dependency is introduced in numerical solution.

Moreover, it should be observed that a very fine mesh must be used to obtain the shape of the damaged zone registered in tests under contact blast loads. This is not the case of more distant explosions characterized by flexure failure that can be modeled with coarser meshes.

A simple correlation between mesh size and erosion limit is used in the paper to obtain similar numerical results. However, this dependency requires further research in order to establish the range of validity and if there are not other variables influencing this problem.

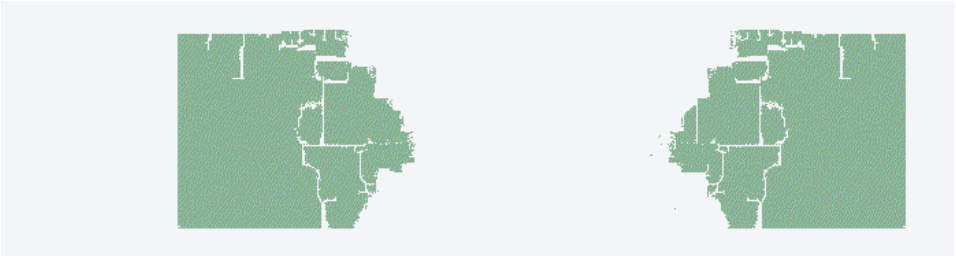

Figure 9: Damaged slab (Numerical simulation 2mm mesh size) $\sigma_1 \geq (\sigma_1)_{\text{lim}} = f_t$

a)

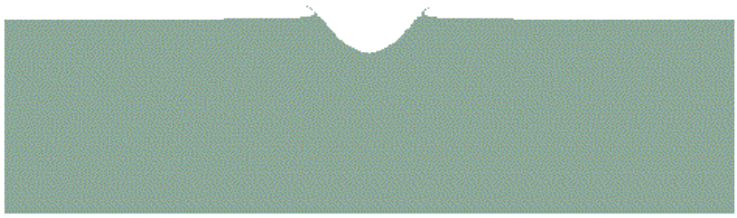

b)

Figure 10: Damaged slab (Numerical simulation 2mm mesh size). Damage failure a) $B = 1.6, D_1 = 0.04,\ D_2 = 1$; b) $B = 0.16, D_1 = 0.004,\ D_2 = 1$

a)

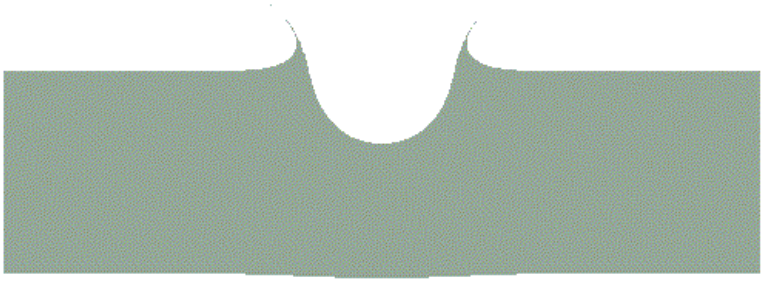

b)

Figure 11: Damaged slab (Numerical simulation 2mm mesh size). $p_{\min} = 0$ failure. a) Failure, b) Plastic zones

AKNOWLEDGEMENTS

The financial support of the CONICET (Argentina) and CIUNT (National University of Tucumán) is gratefully acknowledged.

REFERENCES

ANSYS AUTODYN. Interactive Non-Linear Dynamic Analysis Software, Version 12, User's Manual. *SAS IP Inc*., 2009.

Aráoz G.F. y Luccioni B.M. Curva de fragilidad para muro de mampostería bajo cargas explosivas a partir de simulaciones numéricas. *XX Jornadas Argentinas de Ingeniería Estructural*, 2008.

Beppu M., Miwa K., Itohb M., Katayama M. and Ohno T. Damage evaluation of concrete plates by high-velocity impact. *International Journal of Impact Engineering*, 35: 1419–1426, 2008.

Coughlin A.M., Musselman E.S., Schokker A.J. and Linzell D.G.. Behavior of portable fiber reinforced concrete vehicle barriers subject to blasts from contact charges. *International Journal of Impact Engineering*, 37: 521–529, 2010.

Farnam Y., Mohammadi S. and Shekarchi M. Experimental and numerical investigations of low velocity impact behaviour of high-performance fiber-reinforced cement based composite. *International Journal of Impact Engineering*, 37: 220–229, 2010.

Hao Y., Hao H. and Li Z-X. Confinement effects on impact test of concrete compressive material properties. *International Journal of Protective Structures*, 1(1):145-67, 2010.

Herrmann W. Constitutive equation for the dynamic compaction of ductile porous materials. *Journal Applied Physics*, 40(6):2490–9, 1969.

Islam J., Liu Z. and Swaddiwudhipong S. Numerical study on concrete penetration/perforation under high velocity impact by ogive-nose steel projectile. *Computers and Concrete*, Vol. 8, No. 1, 111-123, 2011.

Lee, E.L. and Tarver, C.M. Phenomenological model of shock initiation in heterogeneous explosives. *Physics of Fluids*, 23(12):2362-2372, 2008.

Lian Y.P., Zhang X., Zhou X. and Ma Z.T. A FEMP method and its application in modeling dynamic response of reinforced concrete subjected to impact loading. *Comput. Methods Appl. Mech. Engrg*. 200: 1659–1670, 2011.

LS-DYNA Keyword user's manual, Version 970. *Livermore Software Technology Corporation*, 2003.

Millard S., Molyneaux T., Barnett S., Gao X. Dynamic enhancement of blast-resistant ultra high performance fibre-reinforced concrete under flexural and shear loading. *International Journal of Impact Engineering* 37: 405–413, 2010.

Nyström U. and Gylltoft K.. Numerical studies of the combined effects of blast and fragment loading. *International Journal of Impact Engineering* 36: 995–1005, 2009.

Nyström U. and Gylltoft K. Comparative numerical studies of projectile impacts on plain and steel-fibre reinforced concrete. *International Journal of Impact Engineering*, 38: 95-105, 2011.

Rabczuk T. and Eibl J. Modelling dynamic failure of concrete with meshfree methods. *International Journal of Impact Engineering,* 32: 1878–1897, 2006.

Riedel, W., Thoma, K. y Hiermaier, S. Numerical analysis using a new macroscopic concrete model for hydrocodes. *Proc. 9th Int. Symposium on Interaction of effects of Munitions with Structures*, 315-322, 1999.

Riedel W., Kawai N. and Kondo K-I. Numerical assessment for impact strength measurements in concrete materials. International Journal of Impact Engineering, 36: 283–293, 2009.

Riedel W, Mayrhofer C., Thoma K. and Stolz A. Engineering and numerical tools for explosion protection of reinforced concrete. *International Journal of Protective Structures*, 1(1): 85-101, 2010.

Shi Y., Li Z-X, Hao H. A new method for progressive collapse analysis of RC frames under blast loading. *Engineering Structures*, 32: 1691-1703, 2010.

Song Z. and Lu Y. Numerical simulation of concrete confined by transverse reinforcement. Computers and Concrete, Vol. 8, No. 1, 23-41, 23 Technical Note, 2011.

Tang E.K.C. and Hao H. Numerical simulation of a cable-stayed bridge response to blast loads, Part I: Model development and response calculations. *Engineering Structures*, 32: 3180-3192, 2010.

Teng T., Chu Y., Chang F., Shen B., Cheng D. Development and validation of numerical model of steel fiber reinforced concrete for high-velocity impact. *Computational Materials Science,* 42: 90–99, 2008.

Tu Z. and Lu Y. Evaluation of typical concrete material models used in hydrocodes for high dynamic response simulations. *International Journal of Impact Engineering*, 36: 132–146, 2009.

Tu Z. and Lu Y. Modifications of RHT material model for improved numerical simulation of dynamic response of concrete. *International Journal of Impact Engineering*, 37: 1072-1082, 2010.

Unosson M. Constitutive equations for concrete materials subjected to high rate of loading. *Linköping Studies in Science and Technology*. Thesis No. 936. LIU-TEK-LIC-2002:09. Department of Mechanical Engineering. Division of Solid Mechanics. Linköpings universitet. Linköping, Sweden, 2002.

Wang Z.L., Konietzky H. and Huang R.Y. Elastic–plastic-hydrodynamic analysis of crater blasting in steel fiber reinforced concrete. *Theoretical and Applied Fracture Mechanics*, 52: 111–116, 2009.

Wang Z.L., Wu J. and Wang J.G. Experimental and numerical analysis on effect of fibre aspect ratio on mechanical properties of SRFC. *Construction and Building Materials*, 24: 559–565, 2010.

Wu K-C, Li B. and Tsai K-C. The effects of explosive mass ratio on residual compressive capacity of contact blast damaged composite columns. *Journal of Constructional Steel Research*, 67: 602-612, 2011.

Xu K and Lu Y., Numerical simulation study of spallation in reinforced concrete plates subjected to blast loading. *Computers and Structures*, 84: 431-438, 2006.

Zhou X.Q., Kuznetsov V.A., Hao H. and Waschl J. Numerical prediction of concrete slab response to blast loading. *International Journal of Impact Engineering,* 35: 1186–1200, 2008.

Zhou X.Q. and Hao H. Mesoscale modelling and analysis of damage and fragmentation of concrete slab under contact detonation. *International Journal of Impact Engineering*, 36: 1315–1326, 2009

Zukas J. Introduction to hydrocodes. *Studies in applied mechanics (Elsevier)* 49, 2004.